Regularizer Performance for SparseCT Image Reconstruction With Practical Subsampling

Matthew J. Muckley*, Baiyu Chen*, Thomas Vahle†, Aaron Sodickson‡, Florian Knoll*,
Daniel K. Sodickson*, and Ricardo Otazo*
*New York University School of Medicine, New York, NY
†Siemens Healthcare GmbH, Erlangen, Germany
‡Harvard Medical School, Boston, MA

***Abstract*—Low-dose X-ray computed tomography (CT) is a major area of research due to the diagnostic capability of CT counterbalanced by the risk of radiation exposure. The standard method for reducing the dose is to decrease the tube current, but this negatively impacts image quality at high dose reduction factors due to photon starvation effects. We investigate an alternative paradigm, called SparseCT, in which a multi-slit collimator (MSC) is placed between the source and the patient. Interrupting the X-ray beam in this way reduces radiation dose to the patient and produces undersampled data from which the image can be estimated using sparse image reconstruction techniques. However, the MSC introduces a number of new considerations, including penumbra effects that require wider slits and more spacing between slits in order to optimize dose efficiency and beam separation. These design choices reduce incoherence in the undersampling scheme and affect the performance of standard edge-preserving/sparsity-promoting regularizers. Here, we simulate these effects in the ideal setting where penumbra effects do not increase the noise in the sinogram. For modest 4-fold retrospective undersampling factors, we observe a slight degradation in an abdominal scan between incoherent-optimal and practical MSC designs for SparseCT. In the future, we plan to use the simulation to inform MSC design prior to fabrication.**

I. Introduction

X-ray computed tomography (CT) is a powerful imaging modality that allows efficient and accurate diagnosis of disease with minimal scanning time. However, CT acquisition utilizes ionizing radiation, which has raised concerns about possible radiation risks. Although in many clinical situations the diagnostic benefit of X-ray CT far outweighs the risk posed by ionizing radiation, the undesirability of ionizing radiation has prompted extensive research into reducing the dose while preserving image quality (e.g., [1]).

The current state-of-the-art approach for reducing ionizing radiation is to decrease the time product of the tube current (measured in milli-Ampere seconds, mAs), which increases noise in the projection data. Reconstruction then proceeds with different statistical models for pre- or post-log sinogram data, usually with regularization. The regularization typically takes on the form of an edge-preserving roughness penalty, similar to Total Variation. A drawback of this approach is that photon starvation effects begin to dominate at high mAs reduction levels. An alternative approach is view-based undersampling (e.g., [2]), where certain angular projections are omitted (analogous to one subset of the canonical ordered subsets algorithm). When combined with edge-preserving or sparsity promoting regularization, view-based subsampling can lead to 9-fold undersampling factors [2], but practical implementation would require being able to quickly turn the source on and off, a feature not available on present CT scanners.

A practical subsampling approach is to use a multi-slit collimator (MSC) to block part of the X-ray flux before it hits the patient as is done in SparseCT [3]. This exposes a subset of detector rows rather than collecting all rows as in the conventional approach. As the gantry rotates around the patient, the MSC would be jittered to expose different rows of the detector, or the X-ray focal spot itself could be moved (a feature present on current X-ray CT systems). A potential benefit of this approach is increased incoherence of the sampling pattern relative to view-based subsampling, a property beneficial for sparsity-promoting regularizers [4]. However, use of an MSC requires further consideration of penumbra effects associated with the non-zero size of the X-ray source [5]. These effects can lead to decrease in the X-ray profile prior to hitting the patient, degrading the SNR of the sinogram. To maintain X-ray fluence, practical MSC design favors larger slit widths, which in turn reduce incoherence.

We explore the maximum performance when using MSC subsampling with standard sparsity-promoting and edge-preserving regularization. We compare the performance of three different classic of regularizers (Total Variation, 3D wavelets, and finite differences with a hyperbola potential) with maximal incoherence and practical collimator designs.

II. Methods

A. Sampling Pattern

Recently, a multi-slit collimator (MSC) was proposed in SparseCT [3] to undersample the projection data by partially blocking the beam as a practical solution to CT undersampling. However, the beam penumbra caused by the finite size of the focal spot can reduce the benefits of undersampling since it reduces the fluence [5]. As such, in MSC design one must

This work was supported by NIH grant U01 EB018760. We would like to thank the Mayo Clinic and grant U01 EB017185 for the data used in this paper.

DOI: 10.12059/Fully3D.2017-11-3108005

balance small slit widths, which are better for incoherence, with the attenuation due to penumbra effects.

Here we examine two configurations for 4-fold undersampling based on the geometry of the Siemens SOMATOM Definition Flash scanner: a W1S4 undersampling, where one out of every four detector rows is open, and W4S16 undersampling, where four rows out of every 16 are open. Both of these methods give a similar dose to the patient, but based on internal simulations, the W1S4 undersampling pattern has a dose efficiency of about one third that of the W4S16 pattern [5]. We would like to identify the magnitude of the coherence drop-off in this sampling regime for a standard set of sparsity-promoting regularizers, so we neglect to consider the effects of decreased X-ray fluence on changing the noise statistics in our retrospectively undersampled experiments. We plan to build more accurate simulations for these effects in the future.

B. Reconstruction Formulation

We consider model-based reconstruction methods that estimate the image by solving an optimization problem:

$$\hat{\mathbf{x}} = \underset{\mathbf{x}}{\operatorname{argmin}} \ \frac{1}{2} \|\mathbf{y} - \mathbf{A}\mathbf{x}\|_2^2 + \beta R(\mathbf{x}), \tag{1}$$

where $R(\mathbf{x})$ is an edge-preserving/sparsity-promoting regularizer. We choose to ignore the standard least-squares weighting for CT due to preprocessing steps applied by the Siemens scanner to our data. We are interested in different forms for the regularizer, $R(\mathbf{x})$, in the context where the paradigm of dose-reduction is changed from the high-noise setting of low tube currents to our setting where we have subsampled data. In principle, with subsampled data and high incoherence, the regularizer should be sparsity-promoting [4].

The most straightforward formulation for an edge-preserving, sparsity-promoting regularizer, $R(\mathbf{x})$, is to use Total Variation:

$$R(\mathbf{x}) = \|\mathbf{C}\mathbf{x}\|_1 , \tag{2}$$

where $\mathbf{C}$ is a finite-differencing matrix. This promotes sparsity, which complies with compressed sensing theory. However, this has the potential drawback of introducing undesirable features such as a salt-and-pepper noise texture at high regularization levels [1].

It can be difficult to achieve very high compression ratios needed for compressed sensing from Total Variation. Based on results in MRI [6], 3D wavelets can give much higher compression ratios than Total Variation. A wavelet-based reconstruction paradigm would use

$$R(\mathbf{x}) = \|\mathbf{W}\mathbf{x}\|_1 , \tag{3}$$

where $\mathbf{W}$ is a wavelet transform. There are many possible wavelet transforms to choose from. One type that leads to an efficient algorithm is to use Daubechies D4 wavelets.

Another alternative to Total Variation that circumvents TV artifacts is to use a regularizer that doesn't promote sparsity for small differences by replacing the absolute value function in (2) with a general potential function:

$$R(\mathbf{x}) = \sum_{k=1}^{K} \psi\left([\mathbf{C}\mathbf{x}]_k\right), \tag{4}$$

where k is the kth output of $\mathbf{C}\mathbf{x}$. There are many choices for $\psi(t)$. We choose the hyperbola, which has been used in other CT applications [2]. The hyperbola function is

$$\psi(t) = \delta^2 \left[\sqrt{1 + (t/\delta)^2} - 1\right], \tag{5}$$

where the δ parameter mediates the tradeoff between the edge-preserving, TV-like properties of the regularizer and the quadratic-like properties of the regularizer.

C. Algorithm Considerations

Each of the above regularizers requires a different algorithm for minimization purposes. All the algorithms used here are of the majorize-minimize class. First, we note the following useful fact from De Pierro [7]:

$$\mathbf{D}_f = \operatorname{diag}\left\{\operatorname{abs}\left(\mathbf{A}^T\right) \operatorname{abs}\left(\mathbf{A}\right) \mathbf{1}\right\} \succeq \mathbf{A}^T\mathbf{A}, \tag{6}$$

which implies that $\mathbf{D}_f$ constructed in this manner is a majorizer for $\mathbf{A}^T\mathbf{A}$. Using the method of separable quadratic surrogates [8], we can then design a surrogate and use it in an optimization algorithm. We design our algorithms without the classic ordered subsets acceleration since our data are already undersampled.

Noting that $\mathbf{D}_f \succeq \mathbf{A}^T\mathbf{A}$, the Total Variation BARISTA algorithm [8] (which is itself a FISTA algorithm [9]) can be applied directly to (1) when $R(\mathbf{x})$ is in the Total Variation form. For the case of orthogonal Daubechies D4 wavelets, we choose to convert the problem into the synthesis form [8], and use FISTA with a Lipschitz constant of $\max(\mathbf{D}_f)$ [9]. For the case of the hyperbola potential function, we use the algorithm of Kim without ordered subsets acceration [10].

III. Experiments

A. Experimental setup

We simulated the proposed MSC sampling scheme at a 4-fold reduction factor by using a retrospectively-undersampled abdominal scan acquired on a Siemens SOMATOM Definition Flash scanner at a volume CT Dose Index (CTDIvol) of 9.27 mGy. We used a central 736 $\times$ 64 $\times$ 4006 (detector channels $\times$ detector rows $\times$ projections) section of the helical sinogram to reconstruct a 768 $\times$ 768 $\times$ 32 image volume (later cropped to 512 $\times$ 512 $\times$ 32) at 0.66 mm $\times$ 0.66 mm $\times$ 3 mm resolution (340 mm $\times$ 340 mm $\times$ 96 mm field of view). The 4-fold reduction factor is modest, but we noticed based on the initialization in Fig. 2 that the images were already quite noisy at this level. All images shown are from slice 20 of the reconstructed image volume. We used two different sampling patterns. The first had one slit open out of every four rows (W1S4), while the second had four slits open out of every 16 rows (W4S16). Fig. 1 shows the two sampling patterns used in the numerical experiments.

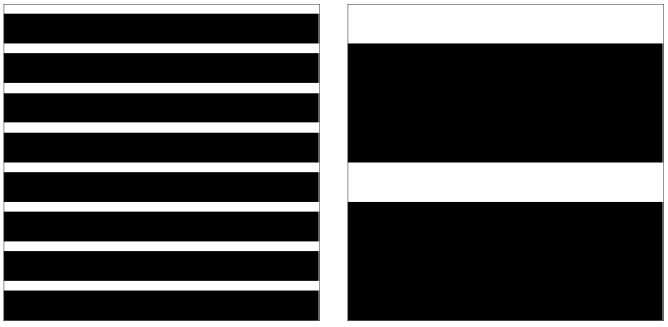

(a) (b)

Fig. 1. MSC sampling patterns used in simulation experiments, where 32 rows of the first 32 channels of a 736×64 detector are shown. (a) shows the W1S4 sampling pattern, while (b) shows the W4S16 sampling pattern.

Each sampling pattern was used on all three regularizers at different regularization strengths, although the images we show are for weaker regularization strengths due to artifacts present with stronger regularization. We chose the regularization parameters based on the visual appeal of the images. All reconstructed images were compared to an unregularized reference image shown in Fig. 2 that was calculated from fully-sampled data. Fig. 3 shows results for all three regularizers in both sampling schemes, while Fig. 4 shows difference images between the results and the reference image in Fig. 2.

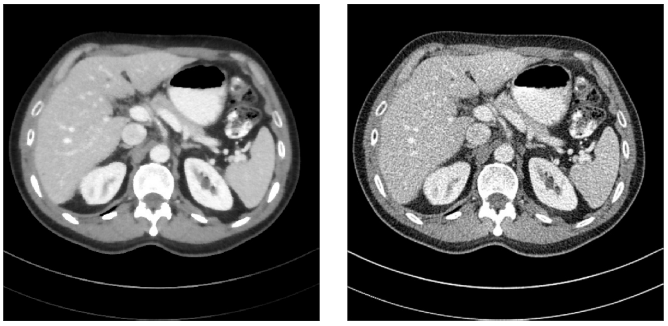

(a) (b)

Fig. 2. (a) A reference image calculated from fully-sampled data. The image is shown in a 40 ± 200 HU abdominal window. (b) A quarter-dose image used to initialize the algorithms.

For these modest undersampling levels, we observed that the main degradation to the initialization images were noise-like artifacts that arise from the incoherence of the sampling pattern. All methods exhibited errors in the location of the edges, with the hyperbola method giving the greatest edge fidelity. The TV images exhibited standard TV features in the reconstructions with flattening of the noise profiles and the introduction of salt-and-pepper noise at higher regularization strengths (results not shown). The wavelet reconstructions performed similar to the TV ones, but introduced artifacts at an earlier stage (results not shown). The 3D orthogonal wavelets also performed more poorly with the W4S16 sampling pattern. Subjectively, we found the hyperbola images blurrier than the others, but we aim to examine this more carefully in the future.

In general, all finite difference reconstructions performed similarly between the W1S4 subsampling scheme and the more practical W4S16. This suggests that in modest undersampling regimes, incoherence reduction from a W1S4 ideal sampling pattern to a W4S16 practical pattern is not significant for finite-difference-based schemes. We aim to examine other MSC designs in the future that facilitate more dramatic sampling factor reductions.

IV. Conclusion

We performed experiments to test a sparsity-based X-ray CT paradigm with retrospective sinogram undersampling to simulate sampling patterns achievable by an MSC design that considers penumbra effects. Our results show that with modest undersampling levels, performance with a practical collimator that considers penumbra effects is slightly less than that that of incoherence-maximal sinogram undersampling in the ideal noise setting. In general, we observed that 3D wavelet reconstructions were artifact-prone in this setting at modest regularization levels. We observed edge location artifacts with the Total Variation regularizer, and the hyperbola introduced some blurriness. In the future we aim to extend these results to more accurately simulate noise in the subsampling case and to build a physical collimator and further test the design principles with measured experimental data. We also plan to explore more advanced regularizer design using principles that incorporate deep learning principles.

References

[1] J.-B. Thibault, K. Sauer, C. Bouman, and J. Hsieh, "A three-dimensional statistical approach to improved image quality for multi-slice helical CT," *Med. Phys.*, vol. 34, no. 11, pp. 4526–44, Nov. 2007.

[2] J. Luo, H. Eri, A. Can, S. Ramani, L. Fu, and B. De Man, "2.5D dictionary learning based computed tomography reconstruction," in *spie-9847*, 2016, p. 98470L.

[3] T. Koesters, F. Knoll, A. Sodickson, D. Sodickson, and R. Otazo, "SparseCT: Interrupted-beam acquisition and sparse reconstruction for radiation dose reduction," in *SPIE Med. Im. 2017*, 2017, to appear.

[4] E. J. Candes and M. B. Wakin, "An introduction to compressive sampling," *IEEE Sig. Proc. Mag.*, vol. 25, no. 2, pp. 21–30, Mar. 2008.

[5] B. Chen, M. J. Muckley, T. O'Donnell, A. Sodickson, T. Flohr, K. Stierstorfer, B. Schmidt, F. Knoll, A. Primak, D. Faul, R. Otazo, and D. Sodickson, "Realistic undersampling model for compressed sensing using a multi-slit collimator," in *Proc. Intl. Mtg. on Fully 3D Image Recon. in Rad. and Nuc. Med*, 2017, submitted.

[6] H. Chandarana, A. M. Doshi, A. Shanbhogue, J. S. Babb, M. T. Bruno, T. Zhao, E. Raithel, M. O. Zenge, G. Li, and R. Otazo, "Three-dimensional MR cholangiopancreatography in a breath hold with sparsity-based reconstruction of highly undersampled data," *Radiology*, pp. 585–94, 2016.

[7] A. R. De Pierro, "A modified expectation maximization algorithm for penalized likelihood estimation in emission tomography," *IEEE Trans. Med. Imag.*, vol. 14, no. 1, pp. 132–7, Mar. 1995.

[8] M. J. Muckley, D. C. Noll, and J. A. Fessler, "Fast parallel MR image reconstruction via B1-based, adaptive restart, iterative soft thresholding algorithms (BARISTA)," *IEEE Trans. Med. Imag.*, vol. 34, no. 2, pp. 578–88, Feb. 2015.

[9] A. Beck and M. Teboulle, "A fast iterative shrinkage-thresholding algorithm for linear inverse problems," *SIAM J. Imaging Sci.*, vol. 2, no. 1, pp. 183–202, 2009.

[10] D. Kim, D. Pal, J.-B. Thibault, and J. A. Fessler, "Accelerating ordered subsets image reconstruction for X-ray CT using spatially non-uniform optimization transfer," *IEEE Trans. Med. Imag.*, vol. 32, no. 11, pp. 1965–78, Nov. 2013.

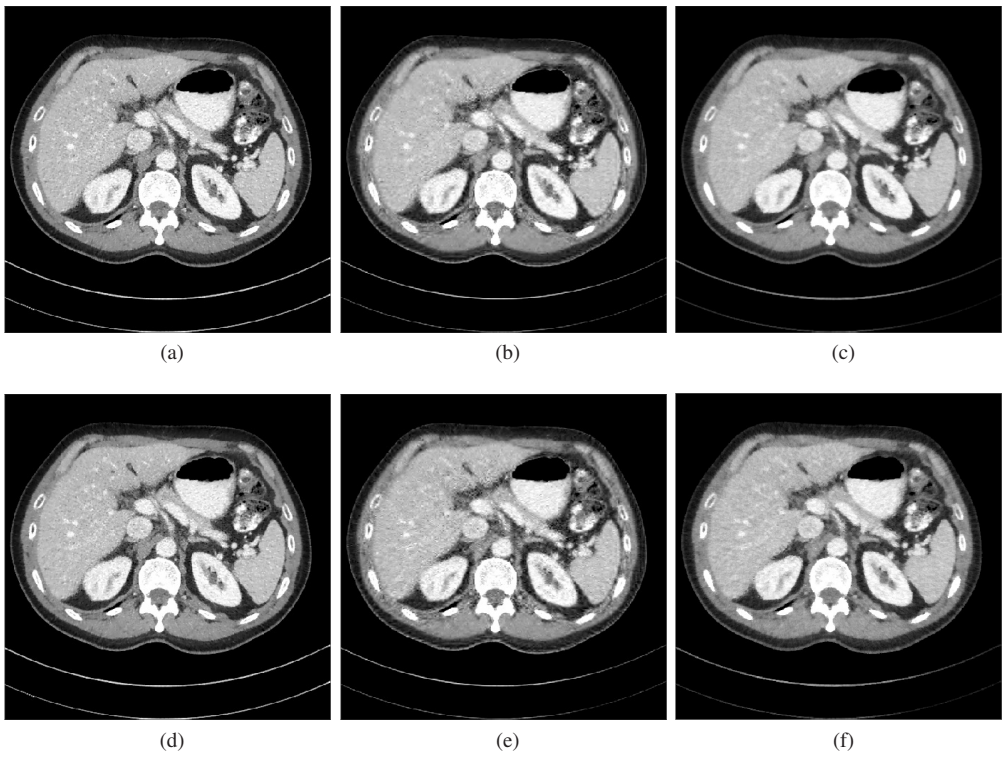

(a) (b) (c)

(d) (e) (f)

Fig. 3. Results of reconstructions. (a), (b), and (c) show the results for Total Variation, orthogonal 3D wavelets, and the hyperbola potential, respectively for the W1S4 sampling pattern. (d), (e), and (f) show the results for Total Variation, orthogonal 3D wavelets, and the hyperbola potential, respectively for the W4S16 sampling pattern. All images are shown with a 40 ± 200 HU abdominal window.

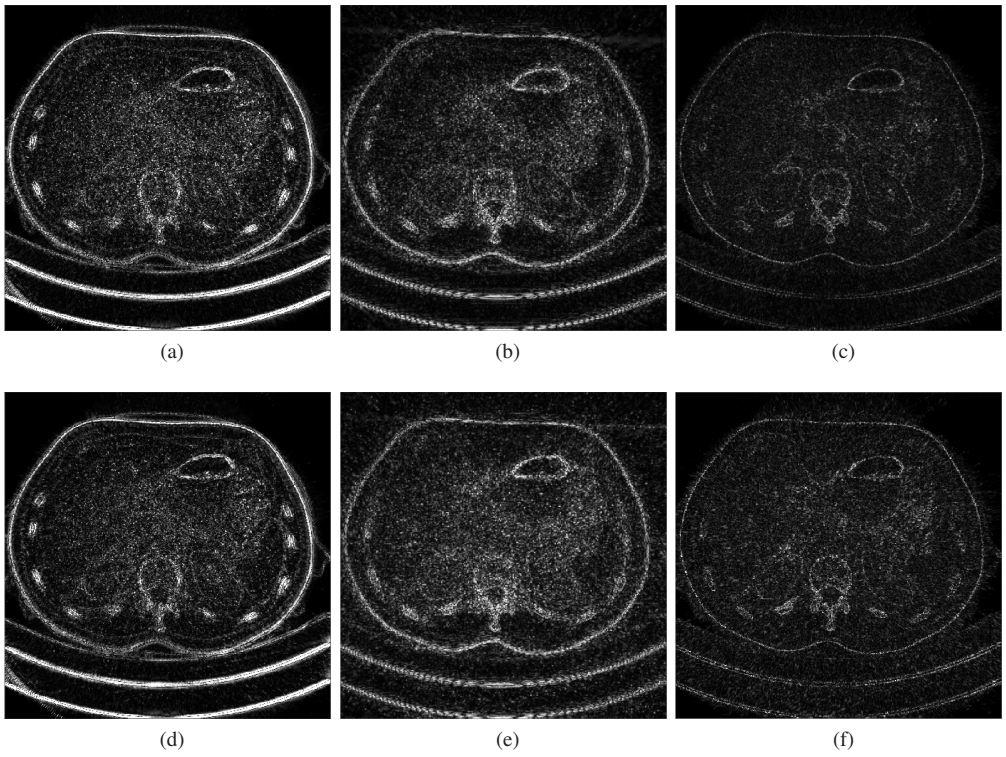

(a) (b) (c)

(d) (e) (f)

Fig. 4. Absolute difference images for the different reconstructions. (a), (b), and (c) show the difference images for Total Variation, orthogonal 3D wavelets, respectively. (d), (e), and (f) show the results for Total Variation, orthogonal 3D wavelets, and the hyperbola potential, respectively. Images are shown with a 50 ± 50 HU viewing window.